The 4th Asian Symposium on Computational Heat Transfer and Fluid Flow, Hong Kong, 3-6 June 2013,
Paper Number: ASCHT0040-T02-1-A

Effect of drop shape on heat transfer during dropwise condensation underneath inclined surfaces

Basant S. Sikarwar[1], K. Muralidhar[1]*, Sameer Khandekar[1]

1: Dept. of Mechanical Engineering, Indian Institute of Technology Kanpur, India
* Correspondent author: kmurli@iitk.ac.in

Abstract

Dropwise condensation underneath a textured surface is a complex multi-scale phenomenon. The instantaneous and time-averaged heat transfer coefficient and wall shear stress depend on several parameters such as the physical and chemical texture of the substrate, thermophysical properties of the fluid, substrate inclination, and interfacial parameters. These factors affect the shape and size of the condensing drops. On an inclined surface, contact angle varies over the three phase contact line and the drop is deformed. Existing models of dropwise condensation approximate the drop shape, usually as a part of the sphere. In the present work, this approximation is relaxed and the shape of the drop is obtained by solving the three dimensional force equilibrium equation. With the shape prescribed, drop-level flow and heat transfer rates associated with fluid motion within have been determined numerically by solving the three dimensional Navier-Stokes and energy equations with applicable boundary conditions. The above information is included at the scale of the dropwise condensation model that proceed from atomic nuclei, to the thermodynamically stable liquid droplets, growth by direct condensation and coalescence, drop instabilities and motion, followed by fresh nucleation. Numerical data obtained from the simulation shows that shape of the drop plays a definite role in the estimation of heat transfer coefficient in dropwise condensation.

Keyword: *Dropwise condensation, Shape of drop, Sliding drops, Wall shear stress, Wall heat flux, Modeling*

1. Introduction

Condensation occurs on the wall when the surface temperature is below the saturation temperature of the adjacent vapor. On specially treated surfaces, liquid droplets will nucleate at specific sites. As condensation proceeds, these droplets grow, coalesce with neighboring drops, and may fall-off or start to slide down the wall. The process is cyclic and drop instability will prevent the formation of a liquid film. Such a phase change process is termed dropwise condensation. It is a heterogeneous phase-change process in which vapor condenses in the form of discrete liquid drops on or underneath a cold substrate. Many investigators have noted that dropwise condensation can be sustained only on specially textured surfaces [1-3]. The heat transfer coefficient during dropwise condensation can be up to an order higher than film condensation. For instance, dropwise was reported to be up to 30 times more effective than filmwise when tested with Langmuir-Blodgett treated surfaces [4-6], and 5~20 times better when a dropwise condensation promotion surface was used [6]. Therefore, dropwise condensation has a strong potential to diminish the size of heat transfer equipment used in thermal and nuclear power plants.

Several researchers [3,8-10] have reported that dropwise condensation is quasi-cyclic process, involving initial nucleation of droplets, growth by direct condensation, coalescence, drop instability and movement, followed by fresh nucleation. Dropwise condensation process depends on the thermophysical properties of the condensing fluid, physico-chemical and thermal properties of the cold substrate, its orientation, surface texture, degree of sub-cooling, thermodynamic saturation conditions and the presence of non-condensable gases. It is a hierarchical process, in the sense that it occurs over a wide range of length and timescales. Close process control of dropwise condensation is difficult and one needs to identify the effect of various parameters on the length and timescales of condensation. As the driving temperature difference for the process is very small, experimental measurement of heat transfer coefficient in dropwise condensation is a challenging task. Leaching of the textured substrate can alter its wettability characteristics and result in aging. Hence, the heat transfer coefficient of dropwise condensation reported in the literature shows considerable scatter [1, 4, 9].

Many researchers have developed mathematical models of dropwise condensation based on a single condensate drop combined with a population model for the entire device [10-13]. There are, however, some

limitations while using this approach. The condensate is assumed to be hemispherical with a circular base. This approximation fails on inclined and variably textured surfaces and is further limited by the fact that drop instability cannot be predicted [14]. The effect of inclination has been accounted for to a limited extent by the two-circle approximation [15-17]. A full calculation wherein the drop shape and its footprint are determined from first principles is yet to be considered within the dropwise condensation model.

The objective of the present study is to determine the drop shape in as much detail as possible within the condensation process underneath a substrate. The shape is used to determine the critical size at which the drop will slide or fall off. Flow and heat transfer within the sliding drop are computed by solving the three dimensional Navier-Stokes and energy equations on an unstructured grid. This information is built into a hierarchical model of dropwise condensation developed by the authors in their previous work [3, 9]. The sensitivity of the model predictions of the instantaneous heat transfer rate to the drop shape is evaluated. The dropwise condensation model proceeds from the atomic scale nuclei, thermodynamically stable liquid droplets, to growth by direct condensation and coalescence, drop instability and motion, followed by fresh nucleation in a cyclic manner.

2. Model development

The overall mathematical model comprises four steps. These are determination of the three dimensional drop shape from a force equilibrium equation, expressions for the critical radius at drop instability, correlations for heat flux and shear stress under a moving drop, and simulation of the overall condensation cycle. Quantities of interest are the condensation patterns, cycle times, area coverage, instantaneous and time-averaged heat fluxes and wall shear stress. The sensitivity of these data to an accurate estimation of drop shape is of primary interest in the present study.

2.1 Estimation of shape of drop underneath an inclined substrate

For a drop sitting on a horizontal surface, the shape is determined by the contact angle and volume, apart from material and interfacial properties. On an inclined surface, the contact angle is replaced by the distribution of angles around the three phase contact line. A variety of approximations have been reported for the contact angle variation, including linear and a cosine functions [16-20]. Elsherbini and Jacobi [22] conducted experiments to investigate the three-dimensional shape of drop on or underneath an inclined surface. Their results show the contact angle variation along the circumference of drop is best fit by a third-degree polynomial in the azimuthal angle. The vertical cross-sectional profile was predicted by the two-circle method sharing a common tangent, while the footprint was approximated by an ellipse. Many researchers [20-24] have argued that the leading and trailing angles of a drop at criticality on or underneath an inclined substrate are equivalent to the advancing and receding contact angles, respectively. Their difference, namely the contact angle hysteresis, is a constant for given liquid-substrate combination. As a consequence, the volume of a liquid drop at criticality will be smaller at higher inclination angles. This overall approach has been adopted in the present study.

The shape of a static drop supported on a solid surface is governed by the Young-Laplace equation that balances weight, surface tension, and the internal pressure [25]. In three dimensions, the equation is difficult to solve and alternative approaches are preferred. A variational approach has been proposed to compute the three-dimensional drop shape, wherein the overall energy of the drop (sum of potential and interfacial energy) is successively minimized. This step has been achieved using Surface-Evolver® [26-27], an open source software. Complete information of the three-dimensional shape and its footprint can be extracted under equilibrium conditions.

The overall numerical methodology is as follows. To initiate the solution, an imaginary cube of liquid of a given volume is taken and its overall energy is minimized to derive the drop shape under equilibrium conditions. In order to provide the surface energy at the solid-liquid interface, the variation of contact angle as a function of the azimuthal angle ϕ, Figure 1(a), needs to be specified. The following contact angle variation proposed in [22] has been adopted:

$$\theta(\phi) = 2\frac{(\theta_{adv} - \theta_{rcd})}{\pi^3}\phi^3 - 3\frac{(\theta_{adv} - \theta_{rcd})}{\pi^2}\phi^2 + \theta_{adv} \tag{1}$$

Here, θ_{adv} is the advancing angle, θ_{rcd} is the receding angle and ϕ is the azimuthal angle, Figure 1(b).The steps for obtaining the shape of three-dimensional non-symmetric drops using Surface-Evolver® are given below.

1. Define an initial cube of liquid with an initial volume equal to V_d.
2. Specify substrate surface inclination, volume constraint and physical parameters.
3. Specify interfacial energy on the solid-liquid contact plane $z = 0$ using the contact angle variation of Eqn. (1), with θ_{adv} and θ_{rcd} , as inputs.
4. Specify gravitational potential energy of the liquid as a function of the plate inclination.
5. Use the gradient descent method of Surface-Evolver® to approach the new three-dimensional drop shape.
6. After each iteration within Surface-Evolver®, correct for the center of the base contour, for calculation of the azimuthal angle ϕ.
7. Repeat steps 3-6 till the drop shape converges.
8. Check for criticality criteria of slide/fall-off

$$\sigma_{lv}\sum_{i=1}^{N}\left(r_b \times d\phi\right)_i \left(\cos\theta\cos\phi\right)_i + V_d \rho g \sin\alpha \le 10^{-6} \tag{2}$$

$$\sigma_{lv}\sum_{i=1}^{N}\left(r_b \times d\phi\right)_i \left(\sin\theta\right)_i + V_d \rho g \cos\alpha \le 10^{-6} \tag{3}$$

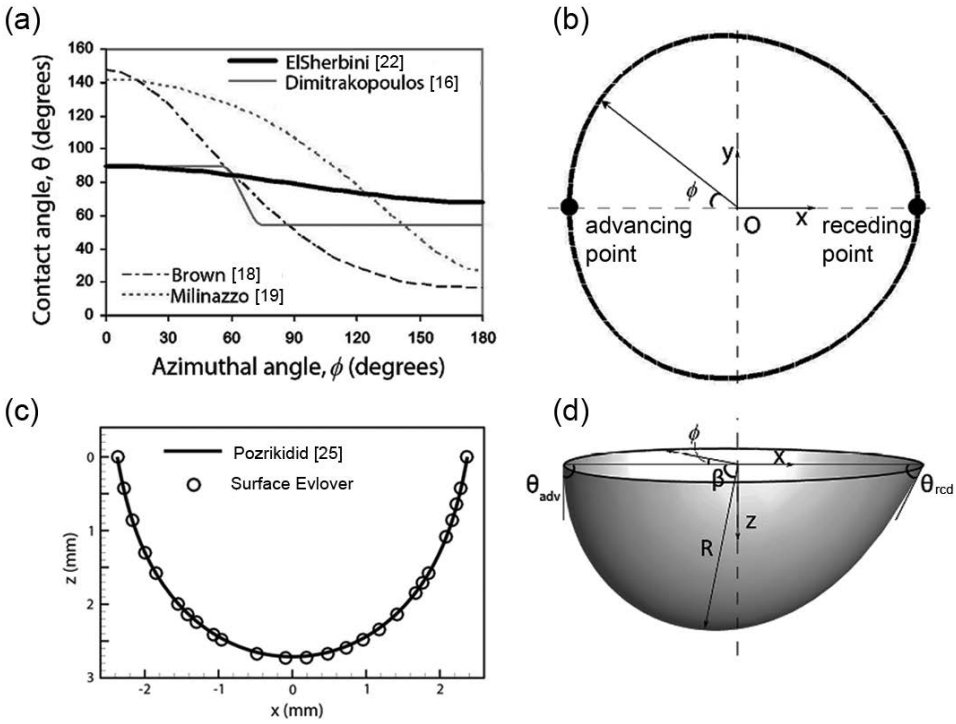

Fig. 1 (a) Contact angle as a function of the azimuthal angle as discussed by El Sherbini and Jacobi[22], Dimitrakopoulos and Higdon [16], Brown et al. [18] and Milinazzo and Shinbrot [19]; (b) Base contour of three-dimensional drop; (c) Validation of the Surface Evolver code for three-dimensional pendant drop shapes. Three-dimensional shape of a 30 μL pendant glycerin drop with a contact angle of 80° is simulated using the Surface Evolver and is compared with the solution of the axisymmetric Young–Laplace equation using the parametric form suggested by Pozrikidis [25]; (d) Numerical simulation of three-dimensional pendant drop showing the azimuthal angle which varies from 0° to 360°, advancing angle θ_{adv}, receding angle θ_{rcd}.

The Surface-Evolver® code was first validated for axisymmetric drops against the axisymmetric form of the Young–Laplace equation. Figure 1(c) compares the shapes of a 30 μL axisymmetric pendant glycerin drop, with a uniform contact angle of 80°, predicted using Surface-Evolver® and the solution of axisymmetric Young–Laplace equation. The match is seen to be quite good. Figure 1(d) presents the simulated shape of a three dimensional glycerin drop underneath an inclined surface.

2.2 Modeling of sliding drop underneath an inclined substrate

Flow and heat transfer are computed within a drop whose shape is obtained from the algorithm of Section 2.1.

The frame of reference for flow and transport calculations is fixed within the liquid drop, the wall moving relative to it at a constant speed. The aim of the simulation is to derive correlations of skin friction coefficient and Nusselt number as a function of Reynolds number and contact angle for various Prandtl number fluids. These correlations serve as input to the overall condensation model of Section 2.3.

The schematic diagram of a three-dimensional deformed drop with an advancing angle θ_{adv} and a receding angle θ_{rcd} is shown in Figure 2(a). The drop is deformed and the difference in angles between the advancing (leading) and receding (trailing) sides is the contact angle hysteresis. Simulations have been carried out with contact angle and hysteresis as parameters varied over 100 to 130° and 5 to 35° respectively, for various substrate inclinations.

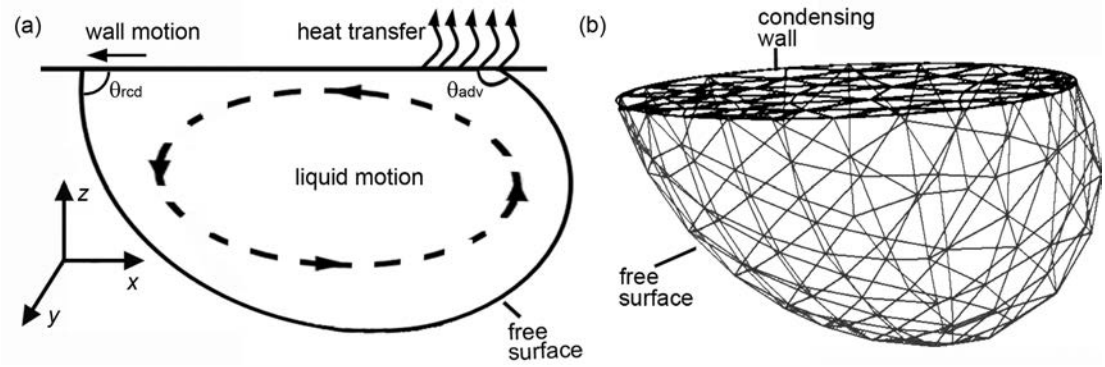

Fig. 2 (a) Schematic diagram of fluid motion and heat transfer at the scale of a single drop; (b) Computational domain with tetrahedral elements in an unstructured grid.

The governing equations for flow and heat transfer within a single drop moving over a solid surface are the incompressible, three dimensional Navier-stokes and energy equations. The governing equations for flow and heat transfer within an incompressible liquid drop are given in Cartesian tensor notation as follows:

$$\frac{\partial u_i}{\partial x_i} = 0 \tag{4}$$

$$\rho\left(\frac{\partial u_i}{\partial t} + u_j \frac{\partial u_i}{\partial x_j}\right) = -\frac{\partial p}{\partial x_i} + \mu \frac{\partial^2 u_i}{\partial x_j^2} \tag{5}$$

$$\rho C_p \left(\frac{\partial T}{\partial t} + u_j \frac{\partial T}{\partial x_j}\right) = k \frac{\partial^2 T}{\partial x_j^2} \tag{6}$$

These equations are written in Cartesian coordinates and solved for the Cartesian velocity components by the finite volume method on an unstructured grid. Boundary conditions are prescribed over the drop surface as follows: At the wall, the no-slip condition holds while the wall has a prescribed temperature. The liquid boundary in contact with vapor is taken to be a stress-free surface. At the free surface, pressure is constant, the normal component of velocity is zero and the shear stress components are also zero. The free surface is also taken to be isothermal at a given distinct saturation temperature. The boundary conditions at the free surface are prescribed in curvilinear coordinates, n being the unit vector in the direction normal to the boundary, while t_1 and t_2 are orthogonal tangential vectors. They need to be transformed from the local curvilinear to Cartesian coordinates during numerical implementation.

The numerical simulation is based on collocated finite volume discretization of the unsteady three-dimensional Navier-Stokes equations over an unstructured mesh. A volume of a single drop is discretized using tetrahedral elements as shown in Figure 2(b). The unstructured mesh is a collection of tetrahedral elements of nearly equal volumes. Pressure-velocity coupling is treated using a smoothing pressure correction method that results in a SIMPLE-like algorithm. Convective terms are discretized by a hybrid upwind scheme. The diffusion terms are discretized using a 2nd order central-difference scheme. Geometry invariant features of the tetrahedral element are used so that the calculation of gradients at cell faces is simplified using nodal quantities of a particular variable. Nodal quantities, in turn, are calculated as a weighted average of the surrounding cell-centered values [29-30]. The discretized system of algebraic equations is solved by the stabilized bi-conjugate gradient method (biCGStab) with a diagonal pre-conditioner. The overall solution algorithm is similar to that proposed by Date [31]. Points of difference are

related to the use of certain invariant properties of the tetrahedral element, powerful linear equations solver as well as a parallel implementation of the computer program [28]. Iterations within the code are run till convergence of 10^{-7} is reached in the residuals. From the velocity and temperature data, wall shear stress and heat transfer rates are determined. The flow and temperature fields are obtained for Reynolds numbers in the range 10-1000 for a range of Prandtl numbers covering liquid metals, water, and organic liquids (Pr ~ 0.005 to 30). Local wall shear stress and local wall heat flux are determined as follows:

$$\left.\begin{aligned} (\tau_{xz})_{wall} &= \mu\left[\frac{\partial u}{\partial z}+\frac{\partial w}{\partial x}\right]_{wall} \\ (\tau_{yz})_{wall} &= \mu\left[\frac{\partial v}{\partial z}+\frac{\partial w}{\partial y}\right]_{wall} \\ \tau_{wall} &= \sqrt{\tau_{xz}^2+\tau_{yz}^2} \end{aligned}\right] \tag{7}$$

$$\left.\begin{aligned} q_{wall} &= -k\left[\frac{\partial T}{\partial n}\right] = -k\left[\frac{\partial T}{\partial z}\right]_{wall} \\ h &= \frac{q_{wall}}{\Delta T} \end{aligned}\right\} \tag{8}$$

The length scale chosen for the analysis is the drop radius at criticality while dimensionless parameters are evaluated at average temperature between the substrate and the drop interface.

2.3 Modeling of complete dropwise condensation

Multiscale modeling of dropwise condensation over textured surfaces has been discussed earlier by the authors [9]. Growth of drops is simulated from drop embryos that grow at specific nucleation sites, while the portion of the surface between the growing drops remains dry. Nucleation sites are randomly distributed on the substrate, while the nucleation site density is a model parameter. The minimum size of the drop can be found from thermodynamic considerations. At the nucleation sites, drops first grow by direct condensation and then coalescence with the neighboring drops. When a certain drop size is reached, body force component exceeds surface tension and the drop is set in motion. The growth rate of drop at each nucleation by direct condensation is limited by the thermal resistance offered by the drop and the substrate in transferring latent heat release to the ambient. The rate of condensation at each nucleation site is estimated by using a quasi-one dimensional approximation for thermal resistances, including the interfacial resistance at the vapor-liquid boundary and conduction resistance through the drop. Drops grow by direct condensation up to a size that is of the order of the distance between adjacent nucleation sites. Beyond this point, coalescence between neighboring drops takes place. Subsequent growth of drops occurs by a combination of direct condensation and coalescence. At the commencement of coalescence, at least two drops will touch each other and are replaced by a drop of equal total volume. The new drop is placed at the resultant center of mass.

Through direct condensation and coalescence, drops are allowed to grow to a critical size where the gravity force exceeds the retention force of surface tension. The drop may then fall-off, for a horizontal substrate, or slide over the inclined substrate. Hidden sites underneath the original drop (and the sweeping area generated by moving drops, for the case of inclined substrates) become active once the droplets fall or slide-off and the entire process is repeated. The equivalent critical radius of the drop at slide-off for an inclined substrate is obtained by Equations 2-3. Equation 2 shows that the r_{crit} is function of substrate orientation, contact angle hysteresis and surface energy.

When the drop achieves terminal velocity, the sum of all external forces acting on it in a direction parallel to inclination of the substrate is zero. These forces are the component of weight parallel to the substrate ($F_{g||}$), surface retention force of the deformed drop due to surface tension (F_r), and wall friction (F_s). Hence

$$F_{g||} + F_r + F_s = 0 \tag{9a}$$

Here, $F_{g||}$ is the component of weight parallel to the inclined substrate; F_r is retention force opposing drop motion and F_s is the viscous force owing to relative velocity between the fluid and the substrate. The terminal velocity can now be calculated as:

$$U = \sqrt{\frac{2(F_{g_{\|}} - F_r)}{C_f \rho A_b}} \tag{9b}$$

As noted, the sliding drop wipes off other drops that lie in its path, exposing fresh area for re-nucleation. In addition, the mass and volume of the drop increase during its passage over the surface, owing to incorporation of smaller drops. The sliding velocity of the drop then needs to be recalculated from Equation (9b). The heat transfer coefficient changes with speed, as will be discussed in succeeding paragraphs. As the drop size increases during sliding, it may reach fall-off criticality at an intermediate time instant. The fall-off criterion can be derived by examining the sum of all forces acting on the drop in the vertical direction. Accordingly, the drop will leave the surface when the stability criteria (Equations 2 and 3) are not satisfied.

Heat transfer during dropwise condensation is calculated by knowing the rate of condensation at the free surface of individual drops located underneath the substrate. The gaps between the growing drops are assumed to be inactive for heat transfer. Heat transfer rate can be determined as follows. The mass of condensate accumulated at the i^{th} nucleation site over a time interval Δt is calculated as:

$$(\Delta m)_i = \rho \frac{\pi}{3}\left(2 - 3\cos\theta_{avg} + \cos^3\theta_{avg}\right)\left(r_{new}^3 - r_{old}^3\right)_i \tag{10}$$

With N, the number of active nucleation sites at given time-step, the average heat transfer coefficient over an area (A) of the substrate during dropwise condensation is:

$$h_{avg} = \frac{h_{lv}}{A\,\Delta T}\frac{\sum_{i=1}^{N}\sum_{j=1}^{K}(\Delta m)_i^j}{t} \quad \text{where } t = \left(\sum_{j=1}^{K}(\Delta t)_j\right) \tag{11}$$

Here, t is the time period of condensation and index $K = (t/\Delta t)$ is the number of time steps.

Next, the formulation for determining the net surface shear stress acting on the condensing surface due to the continuous sliding of drops is described. Shear forces are generated by each drop when it begins sliding after achieving criticality. Thereafter, the mass of the droplet may increase during its travel on the substrate. Thus, shear force is generated by each moving drop, which necessitates spatio-temporal averaging to obtain the average shear stress on the substrate due to the movement of an ensemble of droplets. The average shear stress on the substrate is defined as:

$$\overline{\tau}_s = \frac{\overline{F}_s}{A} = \frac{1}{A}\left[\frac{\sum_{j=1}^{K}\sum_{i=1}^{N}[F_s]_i^j}{t}\right] \tag{12}$$

The average skin friction coefficient on the substrate can then be estimated as:

$$\overline{\overline{C}}_f = \left(\overline{\tau}_s\right)/\left(\tfrac{1}{2}\rho U_{rep}^2\right), \text{where } U_{rep} = \sqrt{g \cdot r_{crit}} \tag{13}$$

Although no droplet motion can commence unless the radius exceeds r_{crit} (either by individual droplet growth by direct condensation or by coalescence), the ensuing terminal velocity of moving drops may vary depending on the path it traverses and the amount of additional mass it gathers due to other droplets on its way. Therefore, representative drop velocity U_{rep} is generically obtained by scaling gravitational acceleration against net kinetic energy of the droplet. All the physico-chemical characteristics of the liquid-solid combination are embedded in the critical radius r_{crit}.

3. Results and Discussion

Results of the present study are reported in three parts: (i) shape of a drop obtained from force equilibrium (called present) compared with the two-circle approximation (previous); (ii) flow and temperature distribution inside an individual sliding drop; and (iii) comparison of dropwise condensation patterns when individual drops are modeled by two different approaches. Figure 3 compares volumes of the drop at criticality for various substrate inclinations. The critical volume determined using Surface-Evolver is higher than the one calculated by the two-circle approximation. Figure 4 shows the shape of the drop obtained from Surface-Evolver as compared to the two-circle approximation. In both methods, the advancing angle is 130° while the contact angle hysteresis is 12°. The predicted shapes are quite distinct while the footprint using the force balance equations is non-circular on inclined substrates.

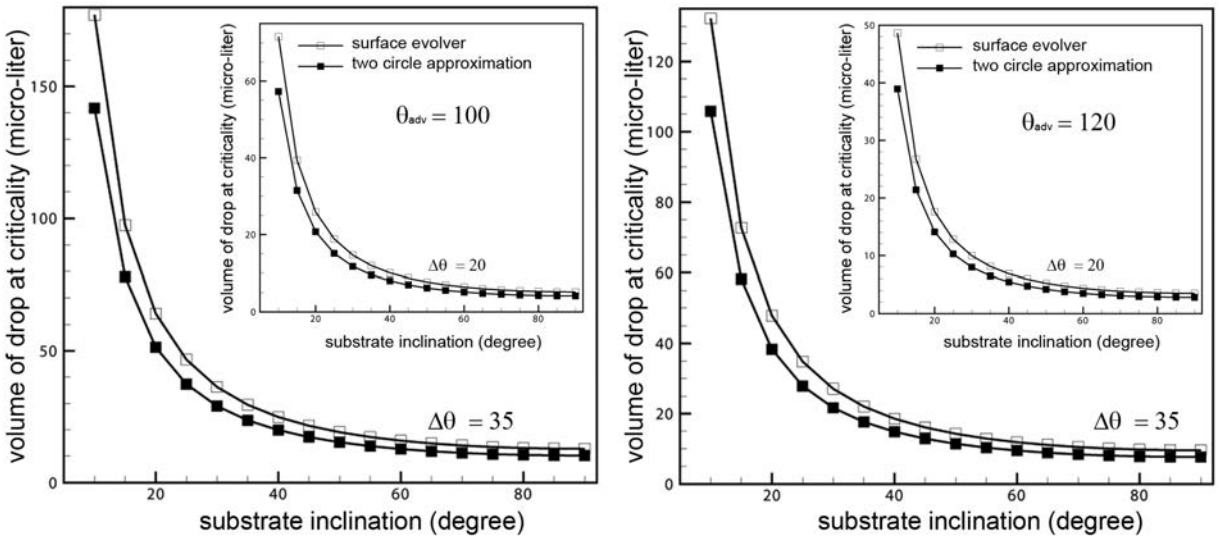

Fig. 3 Variation of volume of water drop at criticality with respect to substrate inclination. (a) Advancing angle = 100°, contact angle hysteresis = 35° while for inset, contact angle hysteresis is 20°. (b) Advancing angle = 120° and contact angle hysteresis = 35° while for the inset, contact angle hysteresis is 20°.

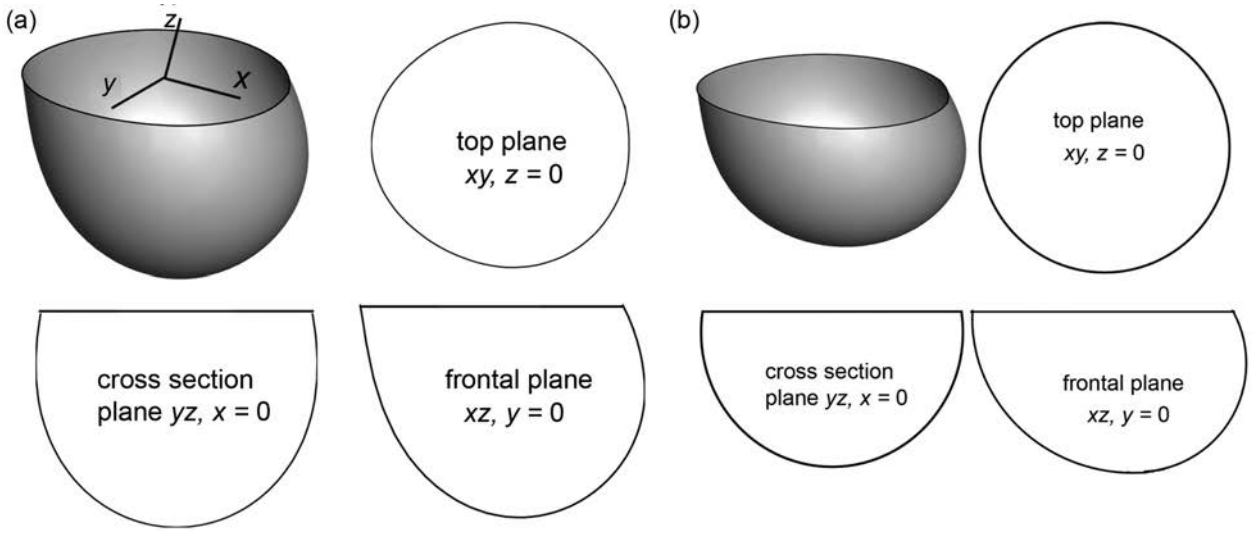

Fig. 4 Isometric view of the shape of a water drop and its two dimensional projections over various planes obtained by (a) Surface Evolver and (b) the two circle approximation. Advancing angle = 130°, contact angle hysteresis = 35°, plate inclination = 45°.

Figure 5(a) shows contours of the *x*-component velocity within a liquid drop at Reynolds numbers of 100 and 500, advancing angle = 130° and contact angle hysteresis = 30°. The surface is inclined at 50° with the horizontal and the drop is located underneath the surface. For the plane selected, the surface motion is to the right, in the plane of the paper. This data for a drop shape determined by the two circle approximation has been reported by the authors elsewhere [28]. The flow distributions, though similar, show minor differences. The velocity magnitude near the free surface is close to the wall speed but in the opposite direction. Temperature contours within water drop over the central plane are shown in Figure 5(b). Temperature gradients at the free surface and the wall are higher compared to the center and clear thermal boundary-layers are formed owing to the small thermal conductivity of water.

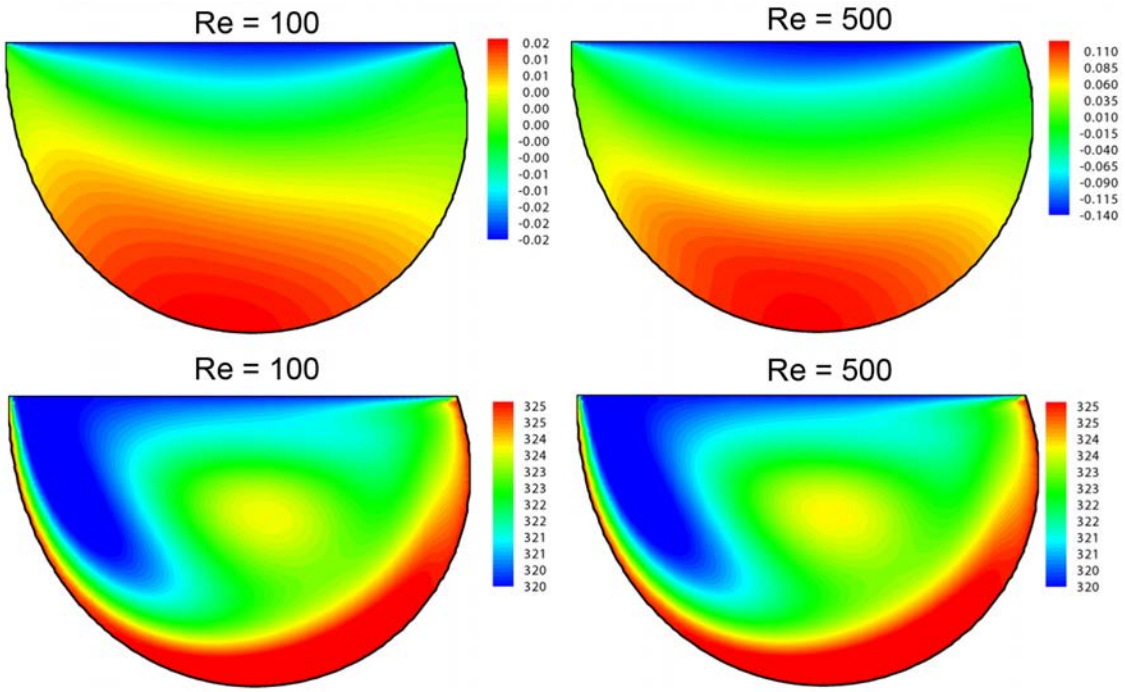

Fig. 5 (a) *x*-component velocity distribution over the frontal $y = 0$ plane on a color scale inside a pendant drop of advancing angle 110°, hysteresis = 20°, plate inclination 45°, Re = 100 and 500. (b) Temperature field inside the deformed drop at Pr = 6 for Reynolds number = 100 and 500.

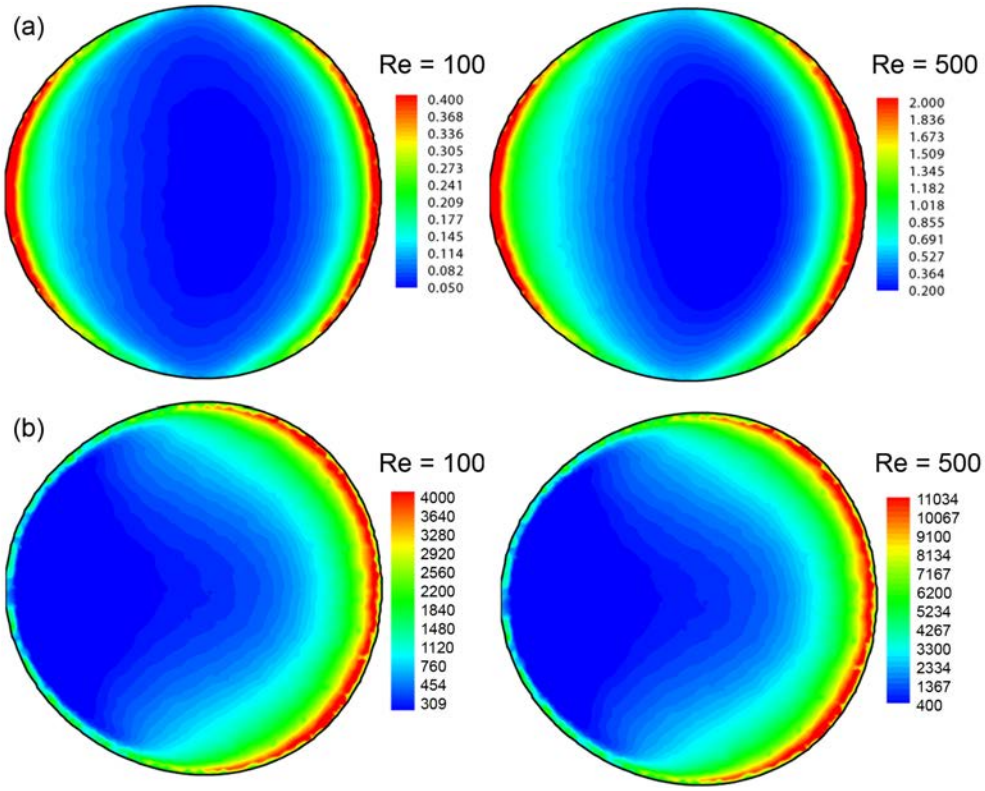

Fig. 6 (a) Wall shear stress and (b) wall heat flux distribution at various Reynolds numbers; Pr=6. Other properties are as in Figure 5.

Distributions of wall shear stress and wall heat transfer are shown in Figures 6(a) and 6(b), respectively. These quantities become quite large near the three-phase contact line of the drop. From the viewpoint of surface wear characteristics, it can be concluded that substrate damage would be initiated along the three phase contact line. Analogous to the wall shear stress, large heat transfer rates are realized in close vicinity of the three-phase contact line as shown in Figure 6(b).

On the basis of the data obtained, the following correlations of average skin friction coefficient and

Nusselt number have been developed in terms of Reynolds number based on the critical radius:

$$\overline{C_f} = 64.2\ \mathrm{Re}^{-0.97}\ \theta_{adv}^{-1.2} \tag{14}$$

$$\left(\overline{\mathrm{Nu}}\right)_{sd} = 12.4\ \mathrm{Re}^{0.196}\ \mathrm{Pr}^{0.1}\ \theta_{avg}^{-0.77} \qquad 3.5 < \mathrm{Pr} < 7 \tag{15}$$

The shape of the drop is brought in as a function of the advance angle and contact angle hysteresis. The skin friction coefficient is correlated with Reynolds number and contact angle. The correlation shows that the skin friction coefficient depends strongly on the advancing angle θ_{adv} (radians), being higher for smaller values. The near reciprocal dependence on Reynolds number shows fully developed flow behavior analogous to internal geometries rather than the boundary-layer flow behavior, seen in external flows. The dependence of the average heat transfer coefficient on Reynolds number is consistently seen to be mild. The sharp dependence of heat transfer on the drop shape is again brought out by Equation 15, through the contact angle. Equations 16-17 have a regression coefficient of better than 99.1%. Correlations similar to Equations 14 and 15 are reported in [28] based on the 2-circle approximation.

3.1 Condensation patterns

The spatio-temporal drop distributions from initial nucleation to instability are shown in Figures 7(a-b) for condensation of water vapor over an inclined substrate at 45^o which is characterized as: advancing angle (θ_{adv}) = 110° and contact angle hysteresis ($\Delta\theta$) = 20°. The nucleation site density in these calculations is taken to be 10^6 per cm^2 while the saturation temperature is 315 K and the degree of subcooling between the vapor and the substrate is 2 K. Figures 7(a-b) show that the average size of the drop in the distribution at a given time in the present approach is slightly higher than the two-circle approximation.

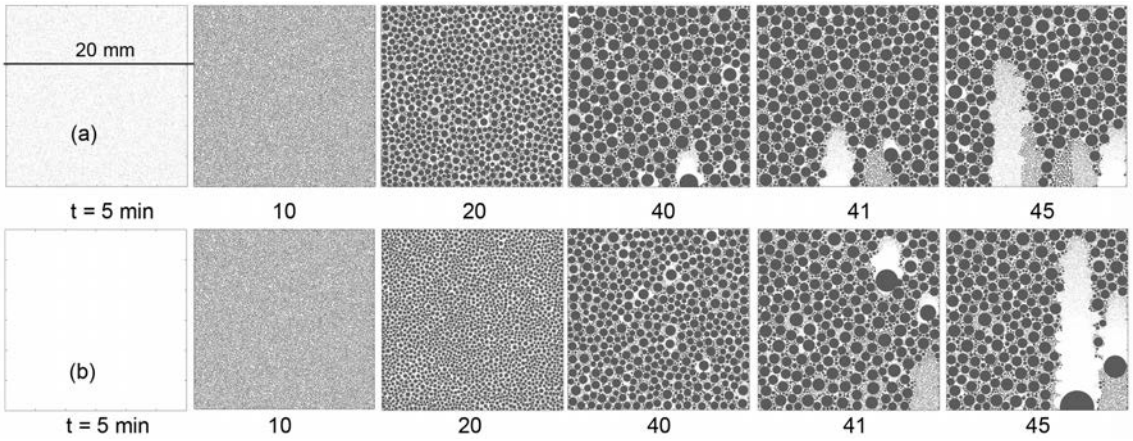

Fig. 7 Drop distributions from initial nucleation to slide-off underneath a surface inclined at 45°; Drop shape determined by (a) Surface-Evolver and (b) 2-circle approximation. Advancing angle 110°, hysteresis = 20^o.

The effect of drop shape and size on area of coverage, available nucleation sites density, wall heat transfer and wall shear stress are summarized in Figure 8. Figure 8(a) shows the area of coverage obtained by the modified approach is higher than the two-circle approximation. Figure 8(a) also shows that the area of coverage decreases as drop slides on the substrate, and can be compared with Figure 7. Figure 8(b) shows the nucleation site density available with respect to time. At an early stage of condensation, it decreases rapidly and reaches a constant value as dynamic state is achieved. Heat transfer through the condensing substrate is presented in Figure 8(c). Heat transfer coefficient obtained with the present approach is less than the two circle approximation because the corresponding drop volume at criticality is greater. Wall shear stresses during drop motion over the condensing substrate are shown in Figure 8(d). The shear stresses determined using the present approach for the drop shape show marginally lower value but depend on the time instant selected within the condensation cycle. Overall, drop size and shape are seen to influence the macroscopic parameters in dropwise condensation.

4. Conclusions

A mathematical model of vapor condensation in the form of drops underneath inclined surfaces is reported. The process starts from nucleation of liquid droplets to direct condensation of vapor, growth by coalescence, and fall-off or slide-off by gravity. At this point, a fresh cycle of condensation is initiated. Shapes of drop underneath inclined surfaces are independently determined. A numerical model based on open domain

software was used to obtain three-dimensional shapes of non-symmetric drops. Drop motion is independently simulated by a 3D Navier-Stokes and energy equations solver. The wall shear stress and heat flux information is included in the condensation model in the form of correlations. The drop size at criticality is determined from a force balance equation and is provided in the model as a correlation. Using this approach, quantities of interest such as drop size at criticality and the average heat transfer rate have been predicted. Numerical data shows that shape of the drop plays a definite role in the estimation of heat transfer coefficient in dropwise contestation. Overall, the proposed approach of using a force equilibrium equation for drop shape yields larger drops at instability, lower heat transfer coefficient and marginally lower wall shear stress, when compared to the 2-circle approximation.

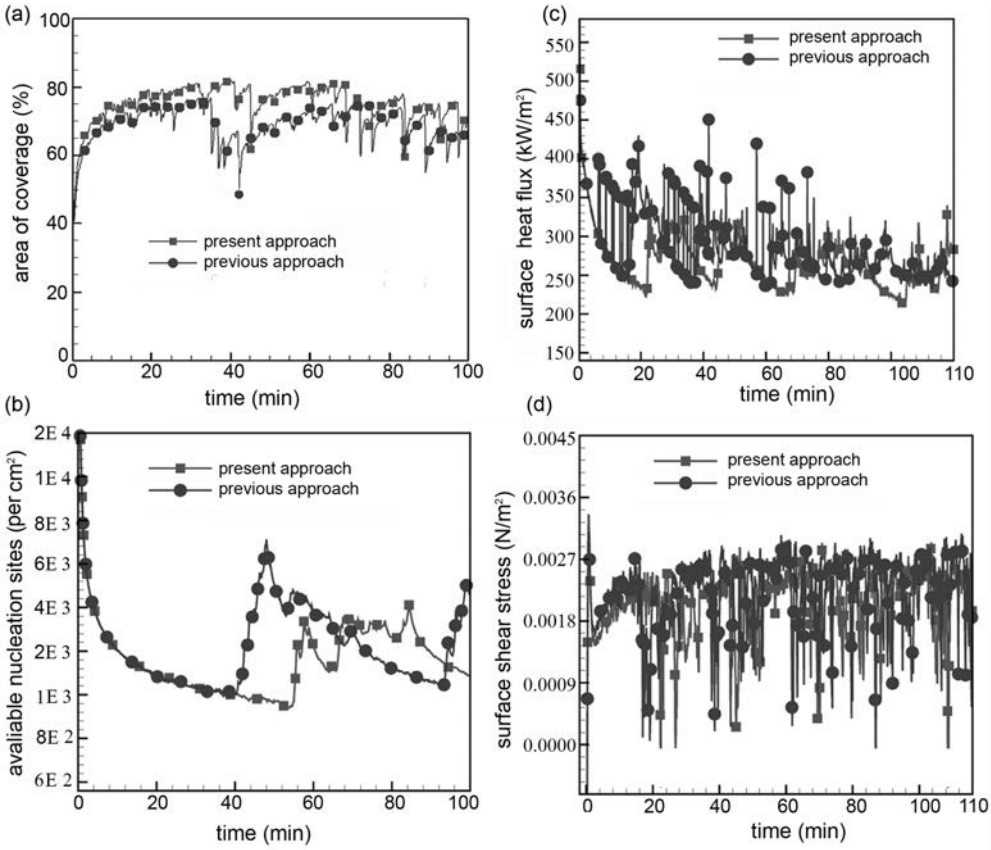

Fig. 8 (a) Variation of area of coverage with respect to time by the present approach compared with the 2-circle approximation [3]; (b) cyclic variation of available nucleation sites with respect to time; (c) cyclic variation of instantaneous wall heat transfer rate during condensation of water vapor, and (d) instantaneous wall shear stress distribution. Surface conditions are as in Figure 7.

References

[1] Rose J. W., "Condensation heat transfer fundamentals", *Chemical Engineering Research and Design*, vol.76, (1998)., pp.143-152

[2] Vemuri S., Kim K.J., Wood B. D., Govindaraju S., and Bell T.W.,"Long term testing for dropwise condensation using self assembled monolayer coatings of n-octadecylmercaptan", *Applied Thermal Engineering*, vol.26(4), (2006), pp. 421-429.

[3] Sikarwar B.S., Battoo N.K., Khandekar S., and Muralidhar K., "Dropwise condensation underneath chemically textured surfaces: simulation and experiments", *ASME J Heat Trans*, vol.133 (2), (2011), pp.21501.

[4] Rose J. W., "Dropwise condensation Theory and experiment: a review", *Proc. Instn. Mech. Engrs.*, vol.216, (2002), pp. 115-128 (2002).

[5] Zhao Q., Zhang D. C,. Lin J. F, and Wang G. M., "Dropwise condensation on L–B film surface", *Chem. Eng. Process*, vol. 35, (1996), pp. 473-477.

[6] Koch G., Kraft K., and Leipertz A., "Parameter study on the performance of dropwise condensation", *Rev. Gen. Therm.*, vol.37,(1998), pp. 539-548.

[7] Rausch M.H., Froba A.P., and A. Leipertz, "Dropwise condensation heat transfer on ion implanted aluminum

surfaces", *Int. J. Heat Mass Trans*, vol.51, (2008), pp. 1061-1070.

[8] Leach R. N., Stevens, F., Langford S. C., and Dickinson J. T., "Dropwise Condensation: Experiments and Simulations of Nucleation and Growth of Water Drops in a Cooling System," *Langmuir*, vol. 22 (2006), pp. 8864-8872.

[9] Sikarwar B. S., Khandekar S., Agrawal S., Kumar S. and Muralidhar K., "Dropwise Condensation Studies on Multiple Scales", Heat *Transfer Engineering*, Special Issue: Advances in Heat Transfer, 33 (3/4), (2012) pp. 301-341.

[10] Carey V. P., "*Liquid–Vapor Phase–Change Phenomena"*, 2nd ed., Hemisphere Publishing Corp., New York, pp. 342-351(1992).

[11] Glicksman R. L., and Hunt W. A., "Numerical simulation of dropwise condensation", *Int. J. Heat Mass Trans*, vol.15, (1972), pp. 2251–2269.

[12] Vemuri S., and Kim K. J., "An Experimental and Theoretical Study on the Concept of Dropwise Condensation", *Int. J. Heat Mass Transfer*, vol. 49, (2006), pp. 649-857.

[13] Tanasawa I., "*Advance in Condensation Heat Transfer,*" in- Advances in Heat Transfer (ed.: Hartnett J. P., Irvine T. F., and Cho I. Y.), vol. 21, (1991), pp. 57-59.

[14] Annapragada S. R., Murthy J. Y. and Garimella S. V., "Droplet retention on an incline", Int *J Heat Mass Trans*, vol. 55, (2012), pp., 1457–1465.

[15] El Sherbini A. I., and Jacobi A. M., "Retention Forces and Contact Angles for Critical Liquid Drops on Non-horizontal Surfaces", *J Colloid Interface Sci*, vol.299, (2006), pp.841-849.

[16] Dimitrakopoulos P. and Higdon J. J. L., "On the gravitational displacement of three-dimensional fluid droplets from inclined solid surfaces", *J Fluid Mech*, vol. 395, (1999), pp.181–209.

[17] Extrand C. W. and Kumagai Y., "Liquid drops on an inclined plane: the relation between contact angles, drop shape, and retentive force." *J Colloid Interface Sci*, vol. 170(2), (1995), pp.515–521.

[18] Brown R. A., Orr Jr F. M., and Scriven L. E., "Static drop on an inclined plate: Analysis by the finite element method", J. *Colloid Interface Sci*, vol. 73(1), (1980), pp.76–87.

[19] Milinazzo F, Shinbrot M., "A numerical study of a drop on a vertical wall", *J Colloid Interface Sci*, vol. 121(1), (1988), pp.254–264.

[20] Korte C. M., and Jacobi, A. M., "Condensation retention effects on the performance of plain-fin and tube heat exchanger: retention data and modeling", ASME *J Heat Trans*, vol.123, (2001), pp.926-936.

[21] Dusan E. B., and Chow R. T. P., "On the ability of drops or bubbles to stick to non–horizontal surfaces of solids", *J Fluid Mech*, vol. 137, (1983), pp. 1–29.

[22] El Sherbini A, I., and Jacobi A. M., "Liquid drops on vertical and inclined surfaces: I. An experimental study of drop geometry." *J Colloid Interface Sci*, vol. 273(2), (2004), pp.556–565.

[23] Cheng P., Li D., Boruvka L., Rotenberg Y. and Neumann A. W., "Automation of axisymmetric drop shape analysis for measurements of interfacial tensions and contact angles", *Colloid Surf* , vol.43, (1990), pp.151–167

[24] Bansal G. D., Khandekar S., Muralidhar K., "Measurement of Heat Transfer during Dropwise Condensation of Water on Polyethylene", *Nanoscale and Microscale Thermophysical Engineering*, vol.13,(2009), pp. 184–201.

[25] Pozrikidis C. "*Fluid dynamics: theory, computation, and numerical simulation*", 2nd edn. Springer, (2009).

[26] Brakke K., "The Surface Evolver", *Exper. Math*, vol. 1(2), (1992), pp.141–165. http://www.susqu.edu/brakke/evolver/evolver.html

[27] Santos M. J., and White J. A., "Theory and simulation of angular hysteresis on planar surfaces", *Langmuir*, vol. 27(24), (2011), pp., 14868–14875.

[28] Sikarwar B. S., Khandekar S., and Muralidhar K., "Simulation of Flow and Heat Transfer in a Liquid Drop Sliding underneath a Hydrophobic Surface", *Int J Heat Mass Trans*, vol.**57** (2), (2013), pp. 786-811.

[29] Barth T. J and Jespersen D. C., "The Design and Application of Upwind Schemes on Unstructured Meshes", *AIAA*, (1989), pp. 89-0366.

[30] Frink N. T., Paresh P. and Shahyar P., "A Fast Upwind Solver for the Euler Equations on Three Dimensional Unstructured Meshes," *AIAA*, (1991), pp. 91-0102.

[31] Date A. W., "Solution of Transport Equations on Unstructured Meshes with Cell Centered Collocated Variables. Part I: Discretization", *Int J Heat Mass Trans*, vol.48, (2005), pp. 1117-1127.